

UCLA

UCLA Previously Published Works

Title

Supramolecular Nanosubstrate-Mediated Delivery for CRISPR/Cas9 Gene Disruption and Deletion

Permalink

<https://escholarship.org/uc/item/0r4559cz>

Journal

Small, 17(28)

ISSN

1613-6810

Authors

Ban, Qian
Yang, Peng
Chou, Shih-Jie
[et al.](#)

Publication Date

2021-07-01

DOI

10.1002/smll.202100546

Peer reviewed



HHS Public Access

Author manuscript

Small. Author manuscript; available in PMC 2022 July 01.

Published in final edited form as:

Small. 2021 July ; 17(28): e2100546. doi:10.1002/sml.202100546.

Supramolecular Nanosubstrate-Mediated Delivery for CRISPR/ Cas9 Gene Disruption and Deletion

Qian Ban[#],

School of Life Sciences, Center for Stem Cell and Translational Medicine, Anhui University, Hefei 230601, China

Peng Yang[#],

Department of Molecular and Medical Pharmacology, David Geffen School of Medicine, California NanoSystems Institute (CNSI), Crump Institute for Molecular Imaging (CIMI), University of California, Los Angeles, Los Angeles, California 90095, United States

Shih-Jie Chou,

Department of Medical Research, and Stem Cell Center, Division of Basic Research, Taipei Veterans General Hospital, Institute of Pharmacology, School of Medicine, National Yang-Ming University, No. 155, Sec. 2, Linong Street 112, Taipei, Taiwan

Li Qiao,

School of Life Sciences, Center for Stem Cell and Translational Medicine, Anhui University, Hefei 230601, China

Haidong Xia,

School of Life Sciences, Center for Stem Cell and Translational Medicine, Anhui University, Hefei 230601, China

Jingjing Xue,

Department of Molecular and Medical Pharmacology, David Geffen School of Medicine, California NanoSystems Institute (CNSI), Crump Institute for Molecular Imaging (CIMI), University of California, Los Angeles, Los Angeles, California 90095, United States

Fang Wang,

Department of Macromolecular Science, State Key Laboratory of Molecular Engineering of Polymers, Fudan University, Shanghai 200433, China

Xiaobin Xu,

Department of Chemistry and Biochemistry, Department of Bioengineering, Department of Materials Science and Engineering, California NanoSystems Institute (CNSI), University of California, Los Angeles, Los Angeles, California 90095, United States

Na Sun,

hrtseeng@mednet.ucla.edu.

Supporting Information

Supporting Information is available from the Wiley Online Library or from the author.

Department of Molecular and Medical Pharmacology, David Geffen School of Medicine, California NanoSystems Institute (CNSI), Crump Institute for Molecular Imaging (CIMI), University of California, Los Angeles, Los Angeles, California 90095, United States

Ryan Y. Zhang,

Department of Molecular and Medical Pharmacology, David Geffen School of Medicine, California NanoSystems Institute (CNSI), Crump Institute for Molecular Imaging (CIMI), University of California, Los Angeles, Los Angeles, California 90095, United States

Ceng Zhang,

Department of Molecular and Medical Pharmacology, David Geffen School of Medicine, California NanoSystems Institute (CNSI), Crump Institute for Molecular Imaging (CIMI), University of California, Los Angeles, Los Angeles, California 90095, United States

Athena Lee,

Department of Molecular and Medical Pharmacology, David Geffen School of Medicine, California NanoSystems Institute (CNSI), Crump Institute for Molecular Imaging (CIMI), University of California, Los Angeles, Los Angeles, California 90095, United States

Wenfei Liu,

Department of Chemistry and Biochemistry, Department of Bioengineering, Department of Materials Science and Engineering, California NanoSystems Institute (CNSI), University of California, Los Angeles, Los Angeles, California 90095, United States

Ting-Yi Lin,

Department of Medical Research, and Stem Cell Center, Division of Basic Research, Taipei Veterans General Hospital, Institute of Pharmacology, School of Medicine, National Yang-Ming University, No. 155, Sec. 2, Linong Street 112, Taipei, Taiwan

Yu-Ling Ko,

Department of Medical Research, and Stem Cell Center, Division of Basic Research, Taipei Veterans General Hospital, Institute of Pharmacology, School of Medicine, National Yang-Ming University, No. 155, Sec. 2, Linong Street 112, Taipei, Taiwan

Petar Antovski,

Department of Molecular and Medical Pharmacology, David Geffen School of Medicine, California NanoSystems Institute (CNSI), Crump Institute for Molecular Imaging (CIMI), University of California, Los Angeles, Los Angeles, California 90095, United States

Xinyue Zhang,

Department of Molecular and Medical Pharmacology, David Geffen School of Medicine, California NanoSystems Institute (CNSI), Crump Institute for Molecular Imaging (CIMI), University of California, Los Angeles, Los Angeles, California 90095, United States

Shih-Hwa Chiou,

Department of Medical Research, and Stem Cell Center, Division of Basic Research, Taipei Veterans General Hospital, Institute of Pharmacology, School of Medicine, National Yang-Ming University, No. 155, Sec. 2, Linong Street 112, Taipei, Taiwan

Chin-Fa Lee,

Department of Chemistry, Research Center for Sustainable Energy and Nanotechnology, Innovation and Development Center of Sustainable Agriculture, National Chung Hsing University (NCHU), 145 Xingda Road, South Dist., Taichung 402, Taiwan

Wenqiao Hui,

Anhui Province Key Laboratory of Livestock and Poultry Product Safety Engineering, Institute of Animal Husbandry and Veterinary Medicine, Anhui Academy of Agriculture Sciences, Hefei 230031, China

Dahai Liu,

School of Stomatology and Medicine, Foshan University, Foshan 528000, China

Steven J. Jonas,

Department of Pediatrics, David Geffen School of Medicine, California NanoSystems Institute (CNSI), Eli & Edythe Broad Center of Regenerative Medicine and Stem Cell Research, Children's Discovery and Innovation Institute, University of California, Los Angeles, Los Angeles, California 90095, United States

Paul S. Weiss,

Department of Chemistry and Biochemistry, Department of Bioengineering, Department of Materials Science and Engineering, California NanoSystems Institute (CNSI), University of California, Los Angeles, Los Angeles, California 90095, United States

Hsian-Rong Tseng

Department of Molecular and Medical Pharmacology, David Geffen School of Medicine, California NanoSystems Institute (CNSI), Crump Institute for Molecular Imaging (CIMI), University of California, Los Angeles, Los Angeles, California 90095, United States

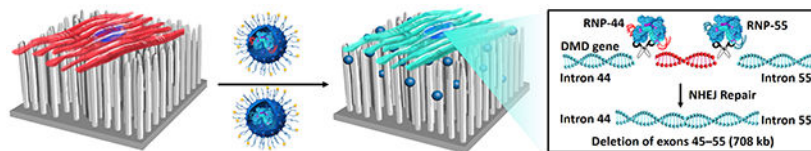
These authors contributed equally to this work.

Abstract

CRISPR/Cas9 is an efficient and precise gene editing technology that offers a versatile solution for establishing treatments directed at genetic diseases. Current CRISPR/Cas9 delivery into cells relies primarily on viral vectors, which suffer from limitations in packaging capacity and safety concerns. To address these issues, we report a nonviral delivery where Cas9•sgRNA ribonucleoprotein (RNP) can be encapsulated into supramolecular nanoparticle (SMNP) vectors to form RNPCSMNPs, which can then be delivered into targeted cells *via* a supramolecular nanosubstrate-mediated delivery (SNMD) strategy. Utilizing the U87 glioblastoma cell line as a model system, we examine a variety of parameters for cellular-uptake of the RNP-laden nanoparticles. We further examine dose-dependent and time-dependent CRISPR/Cas9-mediated gene disruption in a green fluorescent protein (GFP)-expressing U87 cell line (GFP-U87). Finally, we demonstrate the utility of this optimized SMNP formulation in co-delivering Cas9 protein and two sgRNAs that target deletion of exons 45-55 (708 kb) of the dystrophin gene. Mutations in this region lead to Duchenne muscular dystrophy (DMD), a severe genetic muscle wasting disease. We observe efficient delivery of these gene deletion cargoes in a human cardiomyocyte cell line (AC16), induced pluripotent stem cells (iPSCs), and mesenchymal stem cells (MSCs).

Graphical Abstract

A supramolecular nanosubstrate-mediated delivery (SNMD) strategy is developed to improve the delivery efficiency of Cas9 ribonucleoprotein (RNP) into target cells. This strategy leverages local enrichment of supramolecular nanoparticles (SMNPs) from the surrounding medium onto nanowires via molecular recognition, enabling high-efficient CRISPR/Cas9 gene disruption and deletion. This platform offers a general clinical therapeutic solution for genetic diseases, such as DMD.



Keywords

CRISPR/Cas9; supramolecular nanoparticle; nanosubstrate-mediated delivery; Duchenne muscular dystrophy; gene editing

1. Introduction

The clustered regularly interspaced short palindromic repeats (CRISPR)-associated protein 9 (CRISPR/Cas9) system has rapidly shifted from its natural role as an RNA-guided genetic adaptive immune system in prokaryotes to a robust site-specific gene editing method.^[1] The CRISPR/Cas9 system consists of two critical components, *i.e.*, the Cas9 endonuclease and a short, single-guide RNA (sgRNA), which form a Cas9•sgRNA ribonucleoprotein (RNP) complex.^[2] Based on a simple base-pairing mechanism, the RNP identifies and cuts a targeted DNA in the genome, leading to a double-strand break (DSB) at the specified location.^[3] Endogenous DNA repair mechanisms, *e.g.*, the non-homologous end joining (NHEJ) pathway, lead to insertions or deletions (indels)^[4] that result in gene disruption. Gene disruption *via* CRISPR/Cas9 editing has been frequently applied for knocking down genes in cell lines and animal models.^[5] Alternatively, complete gene knockout can be achieved *via* CRISPR/Cas9-mediated gene deletion, where a pair of sgRNA targeting two ends of a given gene are used in the presence of Cas9 protein to induce two DSBs at the targeted sites where subsequent NHEJ-based DNA repair enables precise removal of the gene. In contrast to gene disruption, CRISPR/Cas9-mediated gene deletion offers a different gene knockdown solution capable of removing a DNA sequence (up to 30 million bp)^[6] associated with monogenetic diseases, *e.g.*, Duchenne muscular dystrophy (DMD)^[7] and Leber congenital amaurosis type 10 (LCA10).^[8]

Although CRISPR/Cas9 strategies have considerable potential for treating a series of diseases, several barriers impede their effective translation into patient care, such as minimizing effects associated with off-target editing, ensuring proper delivery of gene-editing reagents into targeted cells, and the optimization of editing efficiency.^[9] Presently, developing highly efficient intracellular delivery methods remains a major obstacle towards the robust application of CRISPR/Cas9 genome editing strategies both *in vitro* and *in vivo*.^[10] Physical strategies such as microinjection and electroporation have been successfully used to deliver CRISPR/Cas9 reagents intracellularly *via* energetic or physical disruption of

cellular membranes.²¹ However, the decrease in cell viability and the potential for premature cell differentiation pose a challenge to their clinical applications. Viral-based approaches utilizing lentivirus (LV),^[11] adenovirus (AV),^[12] and adeno-associated virus (AAV)^[13] - derived vectors remain the standard choice for the delivery of gene-editing machinery due to their easy construction, good production titer, and high transgene expression.^[10a] However, limitations in packaging capacity in AAV (<4.7 kb)^[14] and concerns over safety related to insertional mutagenesis and immunogenicity associated with viral delivery remain. Significant effort has been devoted to exploring the design and application of non-viral vectors,^[10b, 15] including lipids,^[16] polymers^[17] and nanoparticles^[18] for delivery of CRISPR/Cas9 reagents. The CRISPR/Cas9 system can be introduced as Cas9 DNA plasmid,^[17a, 18b, 19] Cas9 mRNA,^[20] or RNP.^[21] Compared to non-viral methods of delivering Cas9 DNA plasmid and Cas9 mRNA, the direct delivery of RNP represents the most straightforward strategy. In principle, non-viral delivery of RNP has the advantage of rapid gene editing, as it skips the gene transcription and/or translation process. The transient gene editing also leads to reduced off-target activity and avoids the concern of integrating CRISPR genes into the host genome. Since the size of Cas9 protein is as large as ~160 kDa, developing more effective delivery vehicles is critical.^[10b]

Previously, we reported a flexible self-assembled approach for preparing supramolecular nanoparticle (SMNP) vectors^[22] *via* mixing three common molecular building blocks, *i.e.*, adamantane-grafted polyamidoamine dendrimer (Ad-PAMAM), adamantane-grafted poly(ethylene glycol) (Ad-PEG), and β -cyclodextrin-grafted polyethyleneimine (CD-PEI). By leveraging multivalent molecular interactions between β -cyclodextrin (CD) and adamantane (Ad) motifs, modular control over the surface chemistry, sizes, and payloads of the nanoparticles can be easily achieved, offering a versatile playground for various diagnostic imaging^[23] and therapeutic applications.^[24] Inspired by existing substrate-mediated delivery approaches,^[25] we developed a supramolecular nanosubstrate-mediated delivery (SNMD) strategy^[26] to improve the delivery efficiency of SMNP vectors, where Ad-grafted silicon nanowire substrates (Ad-SiNWS) were designed for dynamic assembly and local enrichment of SMNPs. As cells settle onto the substrates, their membranes form intimate contacts with the nanowires and generate transient defects that facilitate intracellular uptake of SMNPs. Moreover, one can carry out multiple rounds of delivery on the same batch of cells *via* sequential additions of SMNPs without regenerating/reloading the substrates after each single use. We hypothesized that this SNMD strategy could be applied to deliver CRISPR/Cas9-based RNP complexes efficiently and show that it offers a robust gene editing solution for a variety of human cell types.

We demonstrate that SNMD facilitates the delivery of Cas9•sgRNA RNPs into cells attached to Ad-SiNWS, enabling both CRISPR/Cas9-mediated gene disruption (Figure 1a) and deletion (Figure 1b). Here RNP complexes are encapsulated into SMNP vectors to form **RNPCSMNPs** *via* a self-assembly approach (Figure 1c). To obtain an optimized formulation of RNPCSMNPs, an enhanced green fluorescent protein (EGFP)-labeled Cas9 protein and sgRNA complex (EGFP-labeled RNP) was employed as a cargo in a quantitative fluorescent imaging study. By conducting small-scale combinatorial screening, an optimal formulation of EGFP-labeled RNPCSMNPs that gave the highest cellular uptake was

identified and subjected to time-dependent imaging studies using the U87 cell line as a model system. The optimal formulation identified was subsequently used to delivering a Cas9 protein and green fluorescent protein (GFP) gene-targeting sgRNA complex (Cas9•sgRNA-GFP, *i.e.*, RNP-GFP) into a GFP-expressing U87 cell line (GFP-U87). The RNP-GFP is designed to disrupt GFP gene expression *via* the introduction of a frameshift mutation resulting from the formation of a CRISPR/Cas9-mediated DSB followed by DNA repair *via* NHEJ (Figure 1a). Finally, we demonstrated the utility of SNMD for the CRISPR/Cas9-mediated large deletion of exons 45-55 (708 kb) of the dystrophin gene in human cells, including cardiomyocytes (AC16), induced pluripotent stem cells (iPSCs), and mesenchymal stem cells (MSCs) (Figure 1b). Approximately 60% of mutations causing DMD, a severe inherited genetic muscle wasting disease, occur within exons 45-55 of the dystrophin gene. Effective gene editing at these locations represents an attractive target for gene therapies.^[27] In addition, given that approximately 90% of DMD patients suffer from cardiomyopathies, the capability to correct cardiomyocytes directly or stem cell-derived products may offer a solution to a primary cause of morbidity and mortality in this population.^[27] It has been demonstrated that CRISPR/Cas9-mediated in-frame deletion of exons 45-55 could produce an internally deleted dystrophin protein, resulting in rescue from the disease phenotype.^[7a-c] Here, a pair of RNP complexes, *i.e.*, Cas9 protein and intron 44-targeting sgRNA complex (RNP-44) and Cas9 protein and intron 44-targeting sgRNA complex (RNP-55), were encapsulated in separate SMNP vectors to form RNP-44CSMNPs and RNP-55CSMNPs, respectively. After deletion of exons 45-55 of the dystrophin gene, the 3' end of intron 44 and the 5' end of intron 55 join together to create a new chimeric intron *via* NHEJ. The T7 endonuclease I (T7E1) assay, polymerase chain reaction (PCR), Sanger sequencing, and quantitative PCR were employed to confirm the precise large deletion of exons 45–55 of the dystrophin gene in AC16, MSC, and iPSC cells.

2. Results and Discussion

2.1. Cell-Uptake Studies of EGFP-Labeled RNP *via* SNMD strategy

By taking advantage of our previous experience in using SMNP vectors for co-encapsulating a transcription factor and a DNA plasmid,^[28] RNPCSMNPs were prepared *via* stoichiometric mixing of the desired RNP complex reagents and four SMNP molecular building blocks (Figure 1c). To identify RNPCSMNP formulations that achieve optimal cell-uptake performance, we applied SNMD to conduct a three-step optimization process. A EGFP-labeled Cas9 protein (EGFP-Cas9, GenScript, New Jersey) and sgRNA complex (EGFP-labeled RNP) was used to monitor the cellular uptake in U87 cells using fluorescence microscopy-based quantitative analysis (Figure 2a). Three batches of EGFP-labeled RNPCSMNPs (Figure 2b) were formulated by systemically modulating i) the weight ratios (wt%) of SMNP to EGFP-labeled RNP (from 100:1 to 100:8), ii) SMNP size (from 110 to 200 nm), and iii) the surface coverage of a membrane penetration peptide, TAT (from 2% to 10%).^[29] For cellular-uptake studies, each batch of EGFP-labeled RNPCSMNPs containing 1.0 μg of EGFP-Cas9 was added to a well (in a 24-well plate), in which an Ad-SiNWS ($1 \times 1 \text{ cm}^2$) was immersed with 1.0 mL of Dulbecco's modified Eagle's medium (DMEM). Due to the supramolecular assembly process, EGFP-labeled RNPCSMNPs were quickly enriched and grafted onto the Ad-SiMWS from the medium.

Prior to settling the cells onto the Ad-SiMWS, U87 cells were synchronized in serum-free DMEM overnight (10 h) to the G0/G1 phases of the cell cycle.^[30] Thereafter, approximately 1×10^5 U87 cells were introduced into each well. The delivery efficiency of EGFP-labeled RNP into U87 cells was quantified by fluorescence microscopy 24 h after treatment. We first evaluated how the weight ratios of SMNPs to EGFP-labeled RNP affect the intracellular delivery performance. As shown in Figure 2b and Figure S1, the highest percentage (47%) of EGFP-positive U87 cells was obtained at a ratio of 100:4. Based on this ratio, we then studied the influence of the sizes of RNPCSMNPs. By adjusting the mixing ratio of Ad-PAMAM and CD-PEI, we were able to obtain EGFP-labeled RNPCSMNPs with varying sizes from 110 to 200 nm as measured by dynamic light scattering (DLS, Figure S2). We found that 120 nm EGFP-labeled RNPCSMNPs showed the best cellular uptake, achieving ~60% EGFP-positive cells (Figure S3). TAT-grafted EGFP-labeled RNPCSMNPs were prepared with TAT coverage ranging between 2% to 10%. EGFP-labeled RNPCSMNPs with 8% TAT exhibited the highest cell-uptake performance up to 75% (Figure S4). We thus identified the formulation that yielded the optimal SMNP configuration of 120 nm EGFP-labeled RNPCSMNPs with 8% TAT coverage. These SMNPs were subsequently used in time-dependent imaging studies to evaluate intracellular trafficking of the gene editing reagents.

Note that after cellular uptake and dynamic disassembly of EGFP-labeled RNPCSMNPs, EGFP-labeled Cas9 protein is expected to traffic into the targeted nucleus to facilitate gene editing. To characterize the transport of EGFP-labeled RNP into cell nuclei using the SNMD strategy, we conducted a time-dependent quantitative imaging study on individual U87 cells under the optimal delivery conditions. Three control conditions, *i.e.*, U87 cells treated with EGFP-labeled RNPCSMNPs (without Ad-SiNWS), U87 cells treated with EGFP-labeled RNP (without SMNP vectors), and U87 cells treated with EGFP-labeled RNP encapsulated using the commercial Lipofectamine CRISPRMAX system were tested in parallel to SNMD treated cells (Figure S5). Our results highlight the critical role of both functional components of the SNMD strategy (*i.e.*, the SMNP vectors and the Ad-SiNWS). Multiple cellular uptake studies were performed in parallel and terminated at 0.5, 1.0, 1.5, 2.0, 3.0, 4.0, 5.0, 6.0, 24, and 48 h after treatment (Figure S6). Figure 2c compiles serial fluorescent micrographs of the U87 cells at 1.5, 3, 24, and 48 h after the treatment with EGFP-labeled RNPCSMNPs *via* SNMD. Figure 2d shows the histograms of single-cell EGFP-labeled Cas9 uptake at the respective times, indicating that the highest cell uptake (92% of EGFP-positive U87 cells) occurred at 3.0 h. Thereafter, slow decay of EGFP-labeled Cas9 accumulation was observed. In parallel, the accumulation of EGFP-labeled Cas9 in cell nuclei was also analyzed. Figure 2e compiles serial fluorescent micrographs of individual U87 cells at 0.5, 1.0, 1.5, 2, 3, 4, 6, and 48 h. Figure 2f shows time-dependent EGFP-labeled Cas9 accumulation in the U87 cells' nuclei, achieving maximum nuclear localization of EGFP-labeled Cas9 at 3 h.

2.2. Characterization

In addition to DLS measurements, scanning electron microscope (SEM) and transmission electron microscope (TEM) imaging were utilized to characterize 8%-TAT-grafted EGFP-labeled RNPCSMNPs, which exhibited the optimal EGFP-Cas9 delivery performance. The

SEM and TEM micrographs showed these nanoparticles possessed homogeneous spherical morphologies with sizes of 120 ± 45 nm (Figures 3a, b, and S7), aligning with our DLS data. The zeta potential of the SMNPs was determined to be 20 ± 5 mV (Figure S8). The electron microscope images of the Ad-SiNWS showed that the lengths and diameters of Ad-SiNWS are *ca.* 5-10 μm and 30-80 nm, respectively (Figures 3c, d, and S9a, b). The assembly of SMNPs onto nanosubstrates (Figure 3e and Figure S9c) and the interactions between SiNWS and cells (Figure 3f and Figure S9d) can also be visualized by SEM, verifying the mechanism of the SNMD strategy.

2.3. CRISPR/Cas9-Mediated GFP Gene Disruption via SNMD strategy

To test the gene-editing capabilities of our SNMD approach, we designed SMNP vectors that enable CRISPR/Cas9-mediated GFP gene disruption (Figure 4a). A GFP-targeting sgRNA (sgRNA-GFP) was designed and synthesized. Using the optimized SMNP formulation and parameters identified earlier, the Cas9•sgRNA-GFP ribonucleoprotein (RNP-GFP) was encapsulated into a SMNP vector to generate RNP-GFPCSMNPs (hydrodynamic sizes = 140 ± 30 nm, see Figure S10). We hypothesized that successful introduction of RNP-GFP into the GFP-U87 cells could disrupt GFP expression as this RNP complex was designed to establish a frameshift mutation *via* the generation of CRISPR/Cas9-mediated DNA DSBs and indel formation upon DNA repair *via* NHEJ.^[31] We first examined how different doses of RNP-GFPCSMNPs affected GFP-disruption performance. The RNP-GFPCSMNPs (containing 0.375, 0.75, 1.5, and 3.0 μg Cas9 protein) was first added to a culture well, in which an Ad-SiNWS (1×1 cm^2) was placed in DMEM (1.0 mL). After settling growth-synchronized GFP-U87 cells onto the RNP-GFPCSMNP-loaded Ad-SiNWS for 48 h, the cells were fixed for DAPI nuclear staining. Residual fluorescence from the GFP-U87 cells on the Ad-SiNWS was then measured and analyzed *via* optical microscopy. Figure 4b displays fluorescent micrographs of the GFP-U87 cells in the presence of different doses of RNP-GFPCSMNPs. Figure 4c summarizes the dose-dependent GFP disruption observed upon delivery of the RNP-GFPCSMNPs, suggesting that the minimum effective dose of Cas9 protein is $1.5 \mu\text{g mL}^{-1}$. Using this minimum effective dose, we carried out time-dependent CRISPR/Cas9-mediated GFP disruption experiments to establish the correlation between GFP signal decay and treatment times. Figure 4d shows fluorescent micrographs of the GFP-U87 cells after settling onto Ad-SiNWS presenting RNP-GFPCSMNPs that were taken serially at 0, 24, 36, 48, 60, 72, and 168 h. Irreversible disruption of the EGFP signal is observed in the GFP-U87 cells from 0 to 168 h in culture (Figure 4e). For fluorescent micrographs (Figure S11a) and histograms of GFP signals (Figure 4f and S11b) of four cell samples (GFP-U87, U87, fresh knockout GFP-U87 for 24 h, and long-term knockout GFP-U87 for 72 h), the cut off value of fluorescence intensity for positive and negative cells was determined to be 350 a.u. After treatment with RNP-GFPCSMNPs for 24 h, the GFP signal was reduced by 2% the threshold. After treatment with RNP-GFPCSMNPs for 72 h, 46% of the treated GFP-U87 cells had fluorescent intensity below 350 a.u. After culturing the GFP-U87 cells for one week, the averaged GFP signal remained at a similar level. In an attempt to examine CRISPR/Cas9-mediated gene disruption in GFP-U87 cells directly, we applied the T7E1 assay to detect indel events associated with the CRISPR/Cas9-mediated gene editing at the genomic DNA level.^[32] Genomic DNA was first extracted from treated GFP-U87 cells and

then the sgRNA-targeted surrounding region was amplified *via* polymerase chain reaction (PCR). T7 endonuclease specifically recognizes and cleaves mismatched DNA amplicons associated with the indel events (Figure 4g). The wild-type amplicon (90 bp) and two characteristic fragments (54 bp and 36 bp) were detected and quantified. The intensity of these DNA fragments was quantified using ImageJ, and the indel efficiency based on the T7E1 assay was found to be ~27% for the RNP-GFPCSMNPs-treated cells. Our functional assay of GFP disruption revealed *ca.* 46% CRISPR/Cas9-mediated gene editing efficiency, whereas the T7E1 assay showed *ca.* 27% efficiency at the genomic DNA level. The apparent discrepancy may be due to limitations in the T7E1 assay, which has been shown to underestimate editing efficiency with a peak signal of 37% on a 50% mix of wildtype and mutant alleles.^[33]

We hypothesized that administering additional RNP-GFPCSMNPs treatments after the GFP-U87 cells settle initially on the Ad-SiNWS could further increase the efficiency of CRISPR/Cas9-mediated GFP gene disruption (Figure 4h–k). To test this hypothesis, we administered two to three treatments every 3 h of our 8% TAT-grafted RNP-GFPCSMNPs (containing 1.5 μ g Cas9 protein) to growth-synchronized GFP-U87 cells cultured on an Ad-SiNWS to maintain a steady supply of RNP-GFP. The cells were cultured for 88 h and then observed *via* fluorescence microscopy. For GFP-U87 cells that received three RNP-GFPCSMNP treatments, less fluorescence was detected (Figure 4j) compared to cells treated only once (Figure 4c) or twice (Figure 4h). Analysis of the fluorescence intensity distribution indicates that the triple treatment group exhibited the highest degree of gene disruption (84%, Figure 4k), compared with the single (46%, Figure 4f) and double (63%, Figure 4i) treatment groups, which suggests that multiple rounds of RNP-GFPCSMNP treatments can be used to enhance CRISPR/Cas9-mediated GFP gene disruption. Interestingly, we found that adding more RNP-GFPCSMNPs (3 μ g/mL *vs.* 1.5 μ g/mL Cas9 protein) failed to reduce the GFP signal further and that the administration of 1.5 μ g/mL SMNP doses twice in series was more effective than a single administration of 3 μ g/mL. Possible reasons for these observations include that: i) the SMNPs interact with components of the plasma membrane or extracellular matrix and enter cells primarily through endocytosis. The size, surface charge, and shape of the SMNPs can impact endocytosis and limit the cell's uptake capacity.^[34] Upon reaching this limit, adding more SMNPs does not lead to increased endocytosis. ii) Adding RNP-GFPCSMNPs (1.5 μ g/mL Cas9 protein) once to the Ad-SiNWS causes SMNPs to reach local saturation on the nanowire substrates, so increased concentrations of SMNPs will not increase the loading capacity of SMNPs on the Ad-SiNWS. iii) Considering the possibility that Cas9 protein will be degraded by the cell to some extent, adding SMNPs twice could maintain an effective concentration of Cas9 protein.

2.4. CRISPR/Cas9-Mediated Deletion of Exons 45–55 of Dystrophin Gene *via* SNMD

After successful demonstration of the SNMD strategy for i) delivery of RNP and ii) GFP gene disruption, we further examined whether this approach could be extended for genomic editing of mutations associated with a genetic disease. We selected DMD, a devastating X-linked muscle disease characterized by progressive muscle degeneration and weakness that affects approximately 1 out of 5000 newborn males, as an initial target for testing.^[35]

Mutations in the dystrophin gene are associated with the disease phenotype. Although DMD is one of the most difficult genetic diseases to treat and dystrophin is the largest gene thus far described in the human genome,^[36] about 60% of DMD-causing mutations occur within exons 45–55 of the dystrophin gene. These mutations often involve one or more exon deletions in the dystrophin gene, disrupting the reading frame of the gene and thus lead to a functional loss of dystrophin expression.^[37] The potential for dystrophin gene modification using the CRISPR/Cas9 system has previously been reported *in vitro* and *in vivo* using viral vector-based methods.^[38] For example, a pair of sgRNAs, *i.e.*, sgRNA-44 and sgRNA-55, was designed and applied to achieve the deletion of exons 45–55. Through NHEJ-mediated repair, the 5′ end of intron 55 and the 3′ end of intron 44 are joined together to create a new chimeric intron, resulting in functional rescue from the dystrophic phenotype.⁶⁶ However, these previous demonstrations relied on viral vectors to deliver the gene editing components, which are limited in terms of cargo packaging capacity and by safety concerns due to potential insertional mutagenesis. To address these safety concerns, we leveraged SNMP for CRISPR/Cas9-mediated deletion of exons 45–55 of the dystrophin gene in human cells, including AC16 cells, MSCs, and iPSCs (Figure 5a).

The AC16 cell line was selected as about 90% of individuals with DMD suffer from cardiomyopathies, which represent the primary source of morbidity and mortality in these patients.⁵⁴ First, two different SMNP vectors were prepared to encapsulate Cas9•sgRNA-44 ribonucleoprotein (RNP-44, targeting introns 44) and Cas9•sgRNA-55 ribonucleoprotein (RNP-55, targeting introns 55), respectively, *i.e.*, 8% TAT-grafted **RNP-44CSMNPs** (hydrodynamic sizes = 120 ± 20 nm, see Figure S12a) and 8% TAT-grafted **RNP-55CSMNPs** (hydrodynamic sizes = 130 ± 25 nm, see Figure S12b). Using our optimized delivery protocol, cells received three sequential treatments at 3 h intervals of the RNP-44CSMNPs and RNP-55CSMNPs (each group containing 1.5 μ g Cas9 protein). Empty SMNP vectors (with no Cas9 protein) and a negative control group (not exposed to SMNPs) were tested in parallel. At 88 h post-treatment, the AC16 cells were harvested to analyze indel production *via* the T7E1 assay. As displayed in Figure 5b, the indel production efficiency of RNP-44CSMNPs and RNP-55CSMNPs was 44.3% for intron 44 (two characteristic fragments are 516 and 387 bp) and 41.2% for intron 55 (two characteristic fragments are 458 and 411 bp), respectively. Furthermore, to test the deletion of exons 44–55, we used PCR to detect the repaired DNA junction. First, the forward primer was designed at –231 bp for the sgRNA-44 targeting sequence, *i.e.*, intron 44, while the reverse primer was designed at +232 bp for the sgRNA-55 targeting sequence, *i.e.*, intron 55. Then, we successfully obtained a 497 bp repaired DNA junction in the test group (RNP-44CSMNPs and RNP-55CSMNPs treatments) by PCR, while no fragment was detected in the control group (Figure 5c). Sanger sequencing (Figure 5d and S13) was employed to analyze the DNA fragment at the repaired junction boundary (red arrow in Figure 5a and d), indicating precise deletion of exons 45–55 (708 kb) of the dystrophin gene in AC16 cells. Next, quantitative PCR (qPCR) analysis (Figure 5e) showed that the deletion efficiency of our system in the AC16 cells was 19.8%, higher than what was achieved using electroporation (15.9%), SMNPs only without Ad-SiNWS (7.5%), commercial transfection reagents Lipofectamine CRISPRMAX (7.5%) or Lipofectamine 3000 (6.0%). Note that the deletion efficiency calculated by qPCR is the ratio of exons 44–55 at the specific splice

junction to the non-edited event sequence. The deletion efficiency does not correspond to achieving the correct edit.

On the other hand, demonstrating effective gene editing in human stem cell populations is more desirable for designing gene therapies directed at DMD.^[39] To test whether our SNMD strategy may be used for these applications, we further carried out CRISPR/Cas9-mediated deletion of exons 45–55 of the dystrophin gene in both human MSCs and iPSCs. Sanger sequencing (Figure S14) was employed to analyze the DNA fragment at the repaired junction boundary, indicating the precise deletion of exons 45–55 (708 kb) of the dystrophin gene in treated MSC and iPSC populations. Furthermore, our platform achieved higher deletion efficiencies in MSCs (16.2%) and iPSCs (2.7%), compared with SMNPs only without Ad-SiNWS (4.2% for MSCs and 1.2% for iPSCs), Lipofectamine CRISPRMAX (4.3% for MSCs and 1.1% for iPSCs) and Lipofectamine 3000 (4.2% for MSCs and 1.1% for iPSCs) treated cells (Figure 5f, g). To address the issues of safety and biocompatibility of our SNMD platform, we measured the proliferation and viability of three cell types, as well as conducted microscopy imaging and alkaline phosphatase (AP) staining post CRISPR/Cas9-mediated gene deletion. Our data (Figure S15) suggest that the SNMD platform had less impact on cell proliferation and viability than electroporation and Lipofectamine CRISPRMAX-treated controls. Optical microscopy analyses (Figure S16) showed that each cell type maintained normal cellular morphology after treatment with SMNP vectors *via* the SNMD strategy, suggesting that the platform is not harmful to the cells. Alkaline phosphatase staining indicate that the platform had no effect on the differentiation potential of the iPSCs.

3. Conclusion

We have successfully demonstrated the feasibility of applying a SNMD-based strategy to deliver Cas9 RNP complexes into target cells, enabling CRISPR/Cas9-mediated gene disruption and deletion. This SNMD strategy leverages local enrichment of RNPCSMNPs from the surrounding medium onto nanowires of Ad-SiNWS. As cells come in contact with the nanostructured substrates, physical interactions between nanowires and cell membranes facilitates the uptake of RNPCSMNPs. In our previous work,^[26c] we reported potential of SNMD-based strategy as an effective delivery platform to knockin the HBB/GFP gene into the AAVS1 locus via homology-directed repair (HDR) pathway in hematologic cells to cure hemoglobinopathies. Here, through co-delivering a pair of RNP complexes, we achieved highly efficient large deletion of exons 45-55 (708 kb) in the dystrophin gene via NHEJ pathway in human adherent cells, including AC16 cells, MSCs, and iPSCs, offering a general clinical therapeutic solution for DMD. This is the longest gene deletion record using non-viral vectors showed in the literatures. Future studies will focus on validating the feasibility of this system to deliver CRISPR/Cas9 systems including RNP, DNA plasmid, and mRNA to correct mutated genes, thus broadening the type of diseases that could be targeted by our approach. To explore the potential *in vivo* applications of this platform, we plan to develop an implantable nanosubstrate that is biodegradable and flexible (*e.g.*, based on polymer nanoneedles) to enable implantation into target organs. This work is currently undergoing in our labs.

4. Methods Section

sgRNA Synthesis:

All sgRNA were synthesized by Synbio Technologies. sgRNA-GFP:
gccguccagcucgaccaggaGUUUUAGAGCUAGAAAUAGCAAGUUAAAAUAAGGCUAGU
CCGUUAUCAACUUGAAAAAGUGGCACCGAGUCGGUGCUUUUUU.

sgRNA-44:

guugaaauaaacuacacacuggGUUUUAGAGCUAGAAAUAGCAAGUUAAAAUAAGGCUA
GUCCGUUAUCAACUUGAAAAAGUGGCACCGAGUCGGUGCUUUUUU.

sgRNA-55:

uguugaugcuauaaauaccaaggGUUUUAGAGCUAGAAAUAGCAAGUUAAAAUAAGGCUA
GUCCGUUAUCAACUUGAAAAAGUGGCACCGAGUCGGUGCUUUUUU.

Synthesis of RNPCSMNPs:

The RNPCSMNPs was prepared *via* self-assembly as follows: Cas9 protein (3.0 µg) and sgRNA (0.6 µg, Molar ratio *ca.* 1:1) RNP complex were added in to a 50 µL PBS mixture with CD-PEI (20 µg) and Ad-PEG (45 µg). Then, the DMSO solution (2.0 µL) containing Ad-PAMAM (7.2 µg) was added into above solution and stirred vigorously at 4 °C for 0.5 h. Finally, the PBS solution (10 µL) of Ad-PEG-TAT (3.6 µg) was added into above mixture and stirred vigorously for at 4 °C for 0.5 h to obtain optimal RNPCSMNPs.

Cell culture:

AC16 cells were kindly provided by the Chinese Academy of Sciences, Shanghai, China. The cells were maintained in Dulbecco's modified Eagle's medium (DMEM, High Glucose) with 10% fetal bovine serum (FBS; HyClone, Logan, UT, USA), 100 units/mL penicillin, and 100 µg/mL streptomycin. The cells were incubated at 37 °C with 5% CO₂ in a humidified chamber and passaged when 60% confluence was reached using a trypsin-EDTA solution (RP01007, NuwaCell, China).

Human MSCs were kindly provided by the Shanghai Institute of Biochemistry and Cell Biology, Chinese Academy of Sciences, Shanghai, China. The MSCs were cultured at 37 °C with 5% CO₂ in DMEM/F12 medium supplemented with 10% FBS, 100 units/mL penicillin, and 100 µg/mL streptomycin. Cells were passaged after reaching 80% confluence using trypsin-EDTA.

Human iPSCs were obtained from NuwaCell. Ltd, China. The iPSCs were seeded on Matrigel-coated plates and cultured at 37 °C with 5% CO₂ in Target medium (RP01020, NuwaCell, China) supplemented with 100 units/mL penicillin, and 100 µg/mL streptomycin. Upon reaching 80% confluence, cells were dissociated using trypsin-EDTA and passaged as single cell suspensions in the presence of the selective Rho-associated protein kinase (ROCK) inhibitor Y27632 (5 µM, HY-10071, MedChemExpress).

Delivery of RNPCSMNPs to human cells via the SNMD strategy:

For U87 cells, GFP-U87 cells, AC16 cells, and MSCs, prior to settling the cells onto Ad-SiMWS, the cells were first synchronized in serum-free medium overnight (10 h) to G0/G1 phases of the cell cycle.^[30] After overnight, the medium was replaced by new serum-containing medium. The RNPCSMNPs (containing 1.5 µg of Cas9 protein in 0.5 mL serum-containing medium) was added to each well of a 24-well plate, where a piece of Ad-SiNWS (1×1 cm²) was placed. Approximately 1×10⁵ cells (in 0.5 mL serum-containing medium) were introduced into each well. The cells were co-incubated with SMNPs for a certain period. Every 48 h, 0.5 mL medium was removed via pipette and then new 0.5 mL serum-containing medium was added to each well. The PBS was added to the control groups. After washing with PBS, the cells on the Ad-SiNWS were fixed with PFA (2%) and then stained with DAPI. Microscopy-based image cytometry was used to detect the deliver performances of different conditions. After different treatments, the cells were harvested and the GFP signal was quantified with fluorescent microscope with a CCD camera (Nikon TE2000S, Japan, exposure time: 200 ms).

For iPSCs, the cells were first synchronized in serum-free Target medium (RP01020, NuwaCell, China) overnight (10 h) to G0/G1 phases of the cell cycle. The RNPCSMNPs (containing 1.5 µg of Cas9 protein in 0.5 mL serum-free medium) was added to each well of a 24-well plate, where a piece of Ad-SiNWS (1×1 cm²) was placed. Approximately 1×10⁵ cells (in 0.5 mL serum-free medium to prevent cell differentiation) were introduced into each well. The cells were co-incubated with SMNPs for a certain period. Every 48 h, 0.5 mL medium was removed via pipette and then new 0.5 mL serum-free medium was added to each well.

Encapsulation efficiency and loading capacity of RNP in the RNPCSMNPs:

The encapsulation efficiency of RNP was calculated based on the ratio of RNP encapsulated into the SMNPs to the total RNP added during the synthesis. A NanoDropTM 2000/c Spectrophotometer was used to compare the Cas9 protein and sgRNA concentrations present in the total solution after synthesizing the nanoparticles and in the supernatant collected following centrifugation of RNP-GFPCSMNPs. The encapsulation efficiency of RNP was 83.5%. By determining the ratio of the weight of the encapsulated Cas9 protein to the total weight of the SMNPs, we calculated the loading capacity of RNP to be 4.5%.

Electroporation:

Generic quartz cuvettes were used for all electroporation experiments. After dissociation with trypsin and neutralization with fresh cell culture medium, AC16 cells were centrifuged for 3 min at 1000g. Cells were then resuspended in 100 µl of the desired buffer (BTXpress Electroporation Buffer), followed by the addition of RNP-44 (containing 1.5 µg Cas9 protein) and RNP-55 (containing 1.5 µg Cas9 protein). The AC16 Cells were then transferred to a sterile 0.2-cm cuvette and electroporated using a Lonza[®] Nucleofector[®] II electroporation system (900V, 30ms, 1 pulse). After electroporation, the transfected cells were gently resuspended in 1 mL of pre-warmed medium and were then seeded in 6-well plates and grown at 37 °C and 5% CO₂.

DNA extraction and polymerase chain reaction (PCR):

After RNPCSMNPs delivery for different times, cells were washed with PBS and replaced with DMEM, and then allowed to grow for 48 h. At this time point, cells were harvested, and genomic DNA was extracted with a commercial QIAamp® DNA Mini Kit (Qiagen, Germany), following the manufacturer's instructions. Then, PCR was conducted to amplify GFP and DMD. The primer sequences were listed as follow:

GFP: forward: 5'-GAGCAAGGGCGAGGAGC-3',

reverse: 5'-CCGGACACGCTGAACTTGTG-3'.

DMD introns-44: forward: 5'-GAGAGTTTGCCTGGACGGA-3',

reverse: 5'-CCTCTCTATACAAATGCCAACGC-3'.

DMD introns-55: forward: 5'-TCCAGGCCTCCTCTCTTTGA-3',

reverse: 5'-CCCTTTTCTTGGCGTATTGCC-3'.

We amplified GFP and DMD with an S1000™ Thermal Cycler (Bio-Rad) under the following PCR conditions: 95°C for 3 min followed by 35 cycles (95°C for 15 s, 58°C for 15 s, and 72°C for 20 s) and 72°C for 3 min. The PCR products run through 1.5% agarose electrophoresis gel.

T7 endonuclease assay:

After amplification, the PCR products were hybridized and digested with a T7 endonuclease 1 mutation detection kit (New England Biolabs, NEB #E3321) assays kit. After incubation at 37 °C for 30 min, the product from the T7E1 assay run through 1.5% agarose electrophoresis gel and the bands were analyzed using a gel imaging instrument (AlphaImager® HP).

The formula for the calculation of indel mutation is below:

$$\% \text{ indel} = 100 \times [1 - (1 - \text{fraction cleaved})^{1/2}],$$

where, fraction cleaved = concentration of digested products / (concentration of digested products + concentration of undigested band).

PCR for exons 44-55 deletion in the DMD gene:

After 88 h post-treatment, the cells were harvested to extract genomic DNA and detect exons 44-55 deletion of DMD by PCR. Primers were designed as follow:

Primer introns-44 forward: 5'-TGCCCTCATCTGTCTTAATCAGTA-3',

Primer introns-55 reverse: 5'-GTGCTGTAGTGCCCGGTT-3'.

Primers were synthesized by Sangon biotech company (Shanghai, China). We amplified the target sequence for deletion with an S1000™ Thermal Cycler (Bio-Rad) under the following PCR conditions: 95°C for 5 min followed by 35 cycles (95°C for 15s, 58°C for 15s, and 72°C for 30s) and 72°C for 3 min. The PCR products were checked on a 1.5% electrophoresis gel. When electrophoresis was completed, a longitudinal slice of the gel was

cut, fixed, and purified to extract DNA using a FastPure Gel DNA Extraction Mini Kit (Vazyme, China). The DNA was sent to Sangon Biotech (Shanghai, China) for sequencing.

Quantitative PCR for exons 44-55 deletion ratio detection:

After 88 h post-treatment, AC16 cells were harvested to extract genomic DNA and detect deletion efficiency of exons 44-55 deletion of DMD by in-out Quantitative PCR assay. Primer 44-55 exons deleted forward: 5'-TGCCCTCATCTGTCTTAATCAGTA-3', reverse: 5'-GTGCTGTAGTGCCCGGTT-3'.

Primer 44-55 exons undeleted forward: 5'-ACTCTGACCATAAAAGCGTGGA-3', reverse: 5'-GTGCTGTAGTGCCCGGTT-3'.

Primers were synthesized by Sangon Biotech (Shanghai, China). The reactions were run on a 5100 real-time Thermal Cycler system (Thermo fisher, USA), under the following conditions: 95 °C for 5 min followed by 40 cycles (95 °C for 10 s, 60 °C for 30 s and 60 °C for 30 s). Data were quantified automatically using the 5100 real-time Thermal Cycler system, and the relative expression was determined using the 2^{-Ct} method.

Cell viability assay:

Cell viability of AC16, MSCs, and iPSCs was evaluated using the CCK-8 assay according to the manufacturer's instructions. Cells were seeded into 96-well plates, CCK-8 (10 μ l) was added to each well and incubated for a further 1.5 h at 37 °C. Optical density (OD) was measured at 450 nm using a microplate reader (SpectraMax i3 Platform, Molecular Devices, Austria).

Supplementary Material

Refer to Web version on PubMed Central for supplementary material.

Acknowledgements

This research was supported by the National Institutes of Health (R21EB016270). SJJ acknowledges support from the NIH Common Fund through a NIH Director's Early Independence Award co-funded by the National Institute of Dental and Craniofacial Research and Office of the Director, NIH Grant DP5OD028181.

References

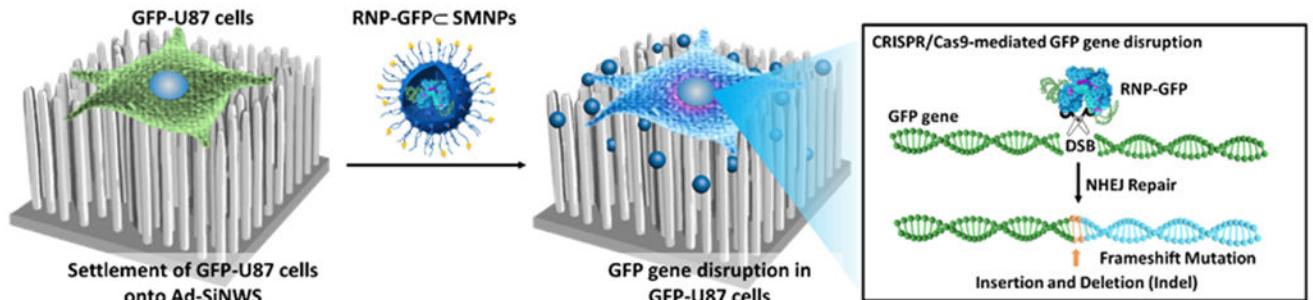
- [1]. a) Ran FA, Hsu PD, Wright J, Agarwala V, Scott DA, Zhang F, Nat. Protoc 2013, 8, 2281 [PubMed: 24157548] b) Doudna JA, Charpentier E, Science 2014, 346, 1258096 [PubMed: 25430774] c) Jiang F, Doudna JA, Annu. Rev. Biophys 2017, 46, 505. [PubMed: 28375731]
- [2]. Nishimasu H, Ran FA, Hsu PD, Konermann S, Shehata SI, Dohmae N, Ishitani R, Zhang F, Nureki O, Cell 2014, 156, 935. [PubMed: 24529477]
- [3]. a) Sternberg SH, Redding S, Jinek M, Greene EC, Doudna JA, Nature 2014, 507, 62 [PubMed: 24476820] b) Sternberg SH, LaFrance B, Kaplan M, Doudna JA, Nature 2015, 527, 110. [PubMed: 26524520]
- [4]. Hsu PD, Lander ES, Zhang F, Cell 2014, 157, 1262. [PubMed: 24906146]
- [5]. a) Yu W, Mookherjee S, Chaitankar V, Hiriyanna S, Kim J-W, Brooks M, Ataeijannati Y, Sun X, Dong L, Li T, Nat. Commun. 2017, 8, 14716 [PubMed: 28291770] b) Wang H, Yang H, Shivalila CS, Dawlaty MM, Cheng AW, Zhang F, Jaenisch R, Cell 2013, 153, 910 [PubMed: 23643243] c) Santiago-Fernández O, Osorio FG, Quesada V, Rodríguez F, Basso S, Maeso D, Rolas L,

- Barkaway A, Nourshargh S, Folgueras AR, Nat. Med. 2019, 25, 423 [PubMed: 30778239] d) Niu Y, Shen B, Cui Y, Chen Y, Wang J, Wang L, Kang Y, Zhao X, Si W, Li W, Cell 2014, 156, 836. [PubMed: 24486104]
- [6]. Essletzichler P, Konopka T, Santoro F, Chen D, Gapp BV, Kralovics R, Brummelkamp TR, Nijman SM, Bürckstümmer T, Genome Res. 2014, 24, 2059. [PubMed: 25373145]
- [7]. a) Long C, Amoasii L, Mireault AA, McAnally JR, Li H, Sanchez-Ortiz E, Bhattacharyya S, Shelton JM, Bassel-Duby R, Olson EN, Science 2016, 351, 400 [PubMed: 26721683] b) Tabebordbar M, Zhu K, Cheng JK, Chew WL, Widrick JJ, Yan WX, Maesner C, Wu EY, Xiao R, Ran FA, Science 2016, 351, 407 [PubMed: 26721686] c) Nelson CE, Hakim CH, Ousterout DG, Thakore PI, Moreb EA, Rivera RMC, Madhavan S, Pan X, Ran FA, Yan WX, Science 2016, 351, 403 [PubMed: 26721684] d) Nelson CE, Wu Y, Gemberling MP, Oliver ML, Waller MA, Bohning JD, Robinson-Hamm JN, Bulaklak K, Rivera RMC, Collier JH, Nat. Med. 2019, 25, 427. [PubMed: 30778238]
- [8]. Maeder ML, Stefanidakis M, Wilson CJ, Baral R, Barrera LA, Bounoutas GS, Bumcrot D, Chao H, Ciulla DM, DaSilva JA, Nat. Med. 2019, 25, 229. [PubMed: 30664785]
- [9]. Lucky SS, Soo KC, Zhang Y, Chem. Rev. 2015, 115, 1990. [PubMed: 25602130]
- [10]. a) Gori JL, Hsu PD, Maeder ML, Shen S, Welstead GG, Bumcrot D, Hum. Gene Ther. 2015, 26, 443 [PubMed: 26068008] b) Wang H-X, Li M, Lee CM, Chakraborty S, Kim H-W, Bao G, Leong KW, Chem. Rev. 2017, 117, 9874. [PubMed: 28640612]
- [11]. Sanjana NE, Shalem O, Zhang F, Nat. Methods 2014, 11, 783. [PubMed: 25075903]
- [12]. Maggio I, Holkers M, Liu J, Janssen JM, Chen X, Goncalves MA, Sci Rep 2014, 4, 5105. [PubMed: 24870050]
- [13]. a) Senís E, Fatouros C, Große S, Wiedtke E, Niopek D, Mueller AK, Börner K, Grimm D, Biotechnol. J 2014, 9, 1402 [PubMed: 25186301] b) Swiech L, Heidenreich M, Banerjee A, Habib N, Li Y, Trombetta J, Sur M, Zhang F, Nat. Biotechnol. 2015, 33, 102. [PubMed: 25326897]
- [14]. Wu Z, Yang H, Colosi P, Mol. Ther. 2010, 18, 80. [PubMed: 19904234]
- [15]. a) Li L, Hu S, Chen X, Biomaterials 2018, 171, 207 [PubMed: 29704747] b) Cai W, Luo T, Mao L, Wang M, Angew. Chem. 2020, 10.1002/ange.202005644.
- [16]. a) Zuris JA, Thompson DB, Shu Y, Guilinger JP, Bessen JL, Hu JH, Maeder ML, Joung JK, Chen Z-Y, Liu DR, Nat. Biotechnol. 2015, 33, 73 [PubMed: 25357182] b) Wang M, Zuris JA, Meng F, Rees H, Sun S, Deng P, Han Y, Gao X, Pouli D, Wu Q, Proc. Natl. Acad. Sci. U. S. A. 2016, 113, 2868. [PubMed: 26929348]
- [17]. a) Li L, Song L, Liu X, Yang X, Li X, He T, Wang N, Yang S, Yu C, Yin T, ACS Nano 2016, 11, 95 [PubMed: 28114767] b) Sun W, Ji W, Hall JM, Hu Q, Wang C, Beisel CL, Gu Z, Angew. Chem. Int. Ed. 2015, 54, 12029c) Liu Q, Zhao K, Wang C, Zhang Z, Zheng C, Zhao Y, Zheng Y, Liu C, An Y, Shi L, Adv. Sci 2019, 6.
- [18]. a) Zhou W, Cui H, Ying L, Yu XF, Angew. Chem. Int. Ed. 2018, 130, 10425b) Wang P, Zhang L, Zheng W, Cong L, Guo Z, Xie Y, Wang L, Tang R, Feng Q, Hamada Y, Angew. Chem. Int. Ed. 2018, 57, 1491c) Lee B, Lee K, Panda S, Gonzales-Rojas R, Chong A, Bugay V, Park HM, Brenner R, Murthy N, Lee HY, Nat. Biomed. Eng. 2018, 2, 497 [PubMed: 30948824] d) Lee K, Conboy M, Park HM, Jiang F, Kim HJ, Dewitt MA, Mackley VA, Chang K, Rao A, Skinner C, Nat. Biomed. Eng. 2017, 1, 889. [PubMed: 29805845]
- [19]. a) Li L, Yang Z, Zhu S, He L, Fan W, Tang W, Zou J, Shen Z, Zhang M, Tang L, Adv. Mater. 2019, 31, 1901187b) Wang N, Liu C, Lu Z, Yang W, Li L, Gong S, He T, Ou C, Song L, Shen M, Adv. Funct. Mater. 2020, 30, 2004940.
- [20]. a) Miller JB, Zhang S, Kos P, Xiong H, Zhou K, Perelman SS, Zhu H, Siegwart DJ, Angew. Chem. Int. Ed. 2017, 56, 1059b) Jiang C, Mei M, Li B, Zhu X, Zu W, Tian Y, Wang Q, Guo Y, Dong Y, Tan X, Cell Res. 2017, 27, 440 [PubMed: 28117345] c) Finn JD, Smith AR, Patel MC, Shaw L, Youniss MR, van Heteren J, Dirstine T, Ciullo C, Lescarbeau R, Seitzer J, Cell Rep. 2018, 22, 2227 [PubMed: 29490262] d) Liu J, Chang J, Jiang Y, Meng X, Sun T, Mao L, Xu Q, Wang M, Adv. Mater. 2019, 1902575e) Cheng Q, Wei T, Farbiak L, Johnson LT, Dilliard SA, Siegwart DJ, Nature Nanotechnol. 2020, 15, 313 [PubMed: 32251383] f) Liu S, Cheng Q, Wei T, Yu, Johnson LT, Farbiak L, Siegwart DJ, Nat. Mater. 2021, 1.

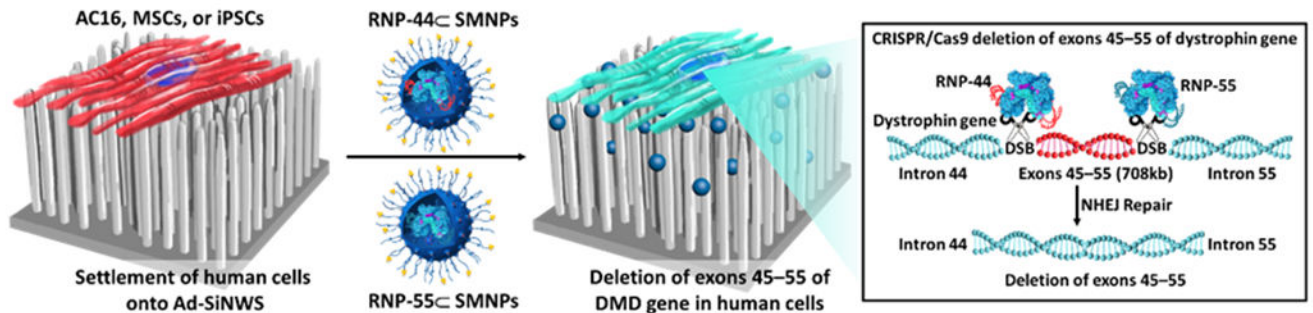
- [21]. a) Gao X, Tao Y, Lamas V, Huang M, Yeh W-H, Pan B, Hu Y-J, Hu JH, Thompson DB, Shu Y, Nature 2018, 553, 217 [PubMed: 29258297] b) Hansen - Bruhn M, de Ávila BEF, Beltrán - Gastélum M, Zhao J, Ramírez - Herrera DE, Angsantikul P, Vesterager Gothelf K, Zhang L, Wang J, Angew. Chem. Int. Ed. 2018, 57, 2657c) Alsaiani SK, Patil S, Alyami M, Alamoudi KO, Aleisa FA, Merzaban JS, Li M, Khashab NM, J. Am. Chem. Soc. 2017, 140, 143 [PubMed: 29272114] d) Pan Y, Yang J, Luan X, Liu X, Li X, Yang J, Huang T, Sun L, Wang Y, Lin Y, Sci. Adv 2019, 5, eaav7199 [PubMed: 30949579] e) Shahbazi R, Sghia-Hughes G, Reid JL, Kubek S, Haworth KG, Humbert O, Kiem H-P, Adair JE, Nat. Mater. 2019, 1f) Wang M, Liu J, Luo T, Xue Y, Mao L, Stang PJ, Angew. Chem. Int. Ed. 2020g) Zhang S, Shen J, Li D, Cheng Y, Theranostics 2021, 11, 614 [PubMed: 33391496] h) Liu C, Wan T, Wang H, Zhang S, Ping Y, Cheng Y, Sci. Adv 2019, 5, eaaw8922 [PubMed: 31206027] i) Wan T, Chen Y, Pan Q, Xu X, Kang Y, Gao X, Huang F, Wu C, Ping Y, J. Control. Release 2020, 322, 236. [PubMed: 32169537]
- [22]. Wang H, Wang S, Su H, Chen KJ, Armijo AL, Lin WY, Wang Y, Sun J, Kamei K. i., Czernin J, Angew. Chem. Int. Ed. 2009, 48, 4344.
- [23]. a) Choi J.-s., Zhu Y, Li H, Peyda P, Nguyen TT, Shen MY, Yang YM, Zhu J, Liu M, Lee MM, ACS Nano 2017, 11, 153 [PubMed: 27997116] b) Chen K-J, Wolahan SM, Wang H, Hsu C-H, Chang H-W, Durazo A, Hwang L-P, Garcia MA, Jiang ZK, Wu L, Biomaterials 2011, 32, 2160. [PubMed: 21167594]
- [24]. a) Choi J.-s., Zhu Y, Li H, Peyda P, Nguyen TT, Shen MY, Yang YM, Zhu J, Liu M, Lee MM, ACS Nano 2016, 11, 153 [PubMed: 27997116] b) Lee JH, Chen KJ, Noh SH, Garcia MA, Wang H, Lin WY, Jeong H, Kong BJ, Stout DB, Cheon J, Angew. Chem. Int. Ed. 2013, 52, 4384c) Wang S, Chen KJ, Wu TH, Wang H, Lin WY, Ohashi M, Chiou PY, Tseng HR, Angew. Chem. Int. Ed. 2010, 49, 3777d) Chou SJ, Yang P, Ban Q, Yang YP, Wang ML, Chien CS, Chen SJ, Sun N, Zhu Y, Liu H, Adv.Sci 2020, 7, 1903432e) Wang F, Yang P, Choi J.-s., Antovski P, Zhu Y, Xu X, Kuo T-H, Lin L-E, Kim DN, Huang P-C, ACS Nano 2018, 12, 6851. [PubMed: 29851454]
- [25]. Wang C-HK, Pun SH, Trends Biotechnol. 2011, 29, 119. [PubMed: 21208672]
- [26]. a) Peng J, Garcia MA, Choi J.-s., Zhao L, Chen K-J, Bernstein JR, Peyda P, Hsiao Y-S, Liu KW, Lin W-Y, ACS nano 2014, 8, 4621 [PubMed: 24708312] b) Hou S, Choi J. s., Chen KJ, Zhang Y, Peng J, Garcia MA, Yu JH, Thakore - Shah K, Ro T, Chen JF, Small 2015, 11, 2499 [PubMed: 25613059] c) Yang P, Chou S-J, Li J, Hui W, Liu W, Sun N, Zhang RY, Zhu Y, Tsai M-L, Lai HI, Sci. Adv 2020, 6, eabb7107. [PubMed: 33097539]
- [27]. Spurney CF, Muscle Nerve 2011, 44, 8. [PubMed: 21674516]
- [28]. a) Liu Y, Du J, Choi J. s., Chen KJ, Hou S, Yan M, Lin WY, Chen KS, Ro T, Lipshutz GS, Angew. Chem. Int. Ed. 2016, 55, 169b) Liu Y, Wang H, Kamei K. i., Yan M, Chen KJ, Yuan Q, Shi L, Lu Y, Tseng HR, Angew. Chem. Int. Ed. 2011, 123, 3114.
- [29]. Wang H, Liu K, Chen K-J, Lu Y, Wang S, Lin W-Y, Guo F, Kamei K.-i., Chen Y-C, Ohashi M, ACS Nano 2010, 4, 6235. [PubMed: 20925389]
- [30]. Golding SE, Rosenberg E, Khalil A, McEwen A, Holmes M, Neill S, Povirk LF, Valerie K, J. Biol. Chem. 2004, 279, 15402. [PubMed: 14744854]
- [31]. Wang M, Zuris JA, Meng F, Rees H, Sun S, Deng P, Han Y, Gao X, Pouli D, Wu Q, Georgakoudi I, Liu DR, Xu Q, Proc. Natl. Acad. Sci. U. S. A. 2016, 113, 2868. [PubMed: 26929348]
- [32]. Schumann K, Lin S, Boyer E, Simeonov DR, Subramaniam M, Gate RE, Haliburton GE, Chun JY, Bluestone JA, Doudna JA, Proc. Natl. Acad. Sci. U. S. A. 2015, 112, 10437. [PubMed: 26216948]
- [33]. Vouillot L, Thélie A, Pollet N, G3: Genes Genom. Genet. 2015, g3. 114.015834.
- [34]. Behzadi S, Serpooshan V, Tao W, Hamaly MA, Alkawareek MY, Dreaden EC, Brown D, Alkilany AM, Farokhzad OC, Mahmoudi M, Chem. Soc. Rev. 2017, 46, 4218. [PubMed: 28585944]
- [35]. Yiu EM, Kornberg AJ, Paediatr J. Child Health 2015, 51, 759.
- [36]. Tennyson CN, Klamut HJ, Worton RG, Nat. Genet. 1995, 9, 184. [PubMed: 7719347]
- [37]. Bushby K, Finkel R, Birnkrant DJ, Case LE, Clemens PR, Cripe L, Kaul A, Kinnett K, McDonald C, Pandya S, Lancet Neurol. 2010, 9, 77. [PubMed: 19945913]

- [38]. a) Long C, McAnally JR, Shelton JM, Mireault AA, Bassel-Duby R, Olson EN, Science 2014, 345, 1184 [PubMed: 25123483] b) Ousterout DG, Kabadi AM, Thakore PI, Majoros WH, Reddy TE, Gersbach CA, Nature Commun. 2015, 6, 6244 [PubMed: 25692716] c) Young CS, Mokhonova E, Quinonez M, Pyle AD, Spencer MJ, J. Neuromuscul Dis. 2017, 1d) Young CS, Hicks MR, Ermolova NV, Nakano H, Jan M, Younesi S, Karumbayaram S, Kumagai-Cresse C, Wang D, Zack JA, Cell Stem Cell 2016, 18, 533. [PubMed: 26877224]
- [39]. Jiang B, Yan L, Wang X, Li E, Murphy K, Vaccaro K, Li Y, Xu RH, Stem Cells 2019, 37, 572. [PubMed: 30561809]

a) CRISPR/Cas9-mediated GFP gene disruption in GFP-U87 cells using the SNMD strategy



b) CRISPR/Cas9-mediated deletion of exons 45–55 of dystrophin gene in human cells using the SNMD strategy



c) Self-assembled synthesis RNP-encapsulated SMNPs, RNP_cSMNPs

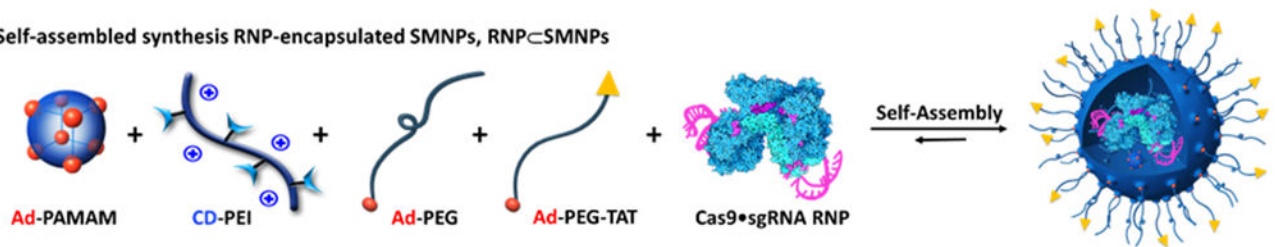
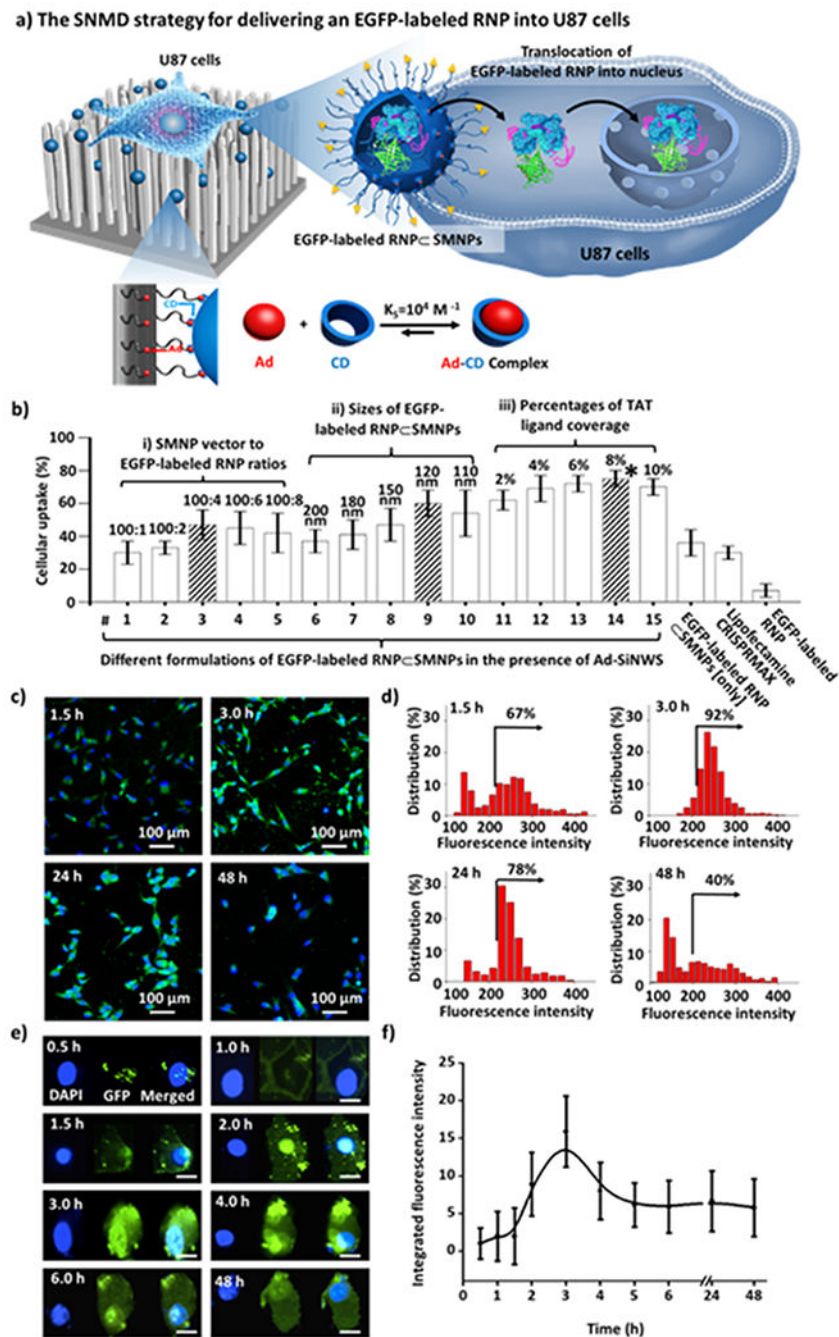


Figure 1.

a) Schematic of the SNMD strategy for CRISPR/Cas9-mediated GFP gene disruption by introducing a Cas9 protein and a GFP-targeting sgRNA (RNP-GFP) into a GFP-U87 cell line. The RNP-GFP cargo is designed to disrupt GFP gene expression by establishing a frameshift mutation *via* the formation of double-strand breaks (DSBs) and subsequent DNA repair *via* the non-homologous end joining (NHEJ) pathway. b) Schematic illustrating the SNMD strategy for CRISPR/Cas9-mediated deletion of exons of 45-55 of dystrophin gene by delivering RNP-44_cSMNPs and RNP-55_cSMNPs into human cells, including cardiomyocytes (AC16), induced pluripotent stem cells (iPSCs), and mesenchymal stem cells (MSCs). After the deletion of exons 45-55 of the dystrophin gene, the 3' end of intron 44 and the 5' end of intron 55 joined together *via* the NHEJ pathway. c) The self-assembled synthesis of RNP_cSMNPs *via* mixing of four SMNP molecular building blocks and RNP cargoes.

**Figure 2.**

a) The SNMD strategy for delivering an EGFP-labeled Cas9 protein and a sgRNA complex (EGFP-labeled RNP) into U87 cells. b) Different formulations of EGFP-labeled RNPCSMNPs were subjected to cellular uptake studies in the presence Ad-SiNWS. An optimal formulation of 120 nm EGFP-labeled RNPCSMNPs with 8% TAT coverage (*) was identified. Three control conditions, *i.e.*, EGFP-labeled RNPCSMNPs [only] (without Ad-SiNWS), EGFP-labeled RNP encapsulated using the commercial Lipofectamine CRISPRMAX system, and EGFP-labeled RNP (without SMNP vectors) were tested. c)

Serial fluorescent micrographs of the U87 cells taken at 1.5, 3, 24, and 48 h after treatment with SMNPs. d) By performing single-cell image analyses to quantify EGFP-labeled Cas9 signals in the micrographs shown in **2c**, histograms of single-cell EGFP-Cas9 uptake were obtained for the respective times. The optimal cell uptake (92% of U87 cells) was observed at 3 h post-treatment. e) Serial fluorescence micrographs of individual U87 cells depict dynamic accumulation of EGFP-labeled Cas9 signals in cell nuclei at 0.5, 1.0, 1.5, 2, 3, 4, 6, and 48 h. All scale bars are 20 μm . f) Time-dependent EGFP--labeled Cas9 accumulation in cell nuclei, which reaches a maximum at 3.0 h. Data are presented as means \pm SD of three independent assays.

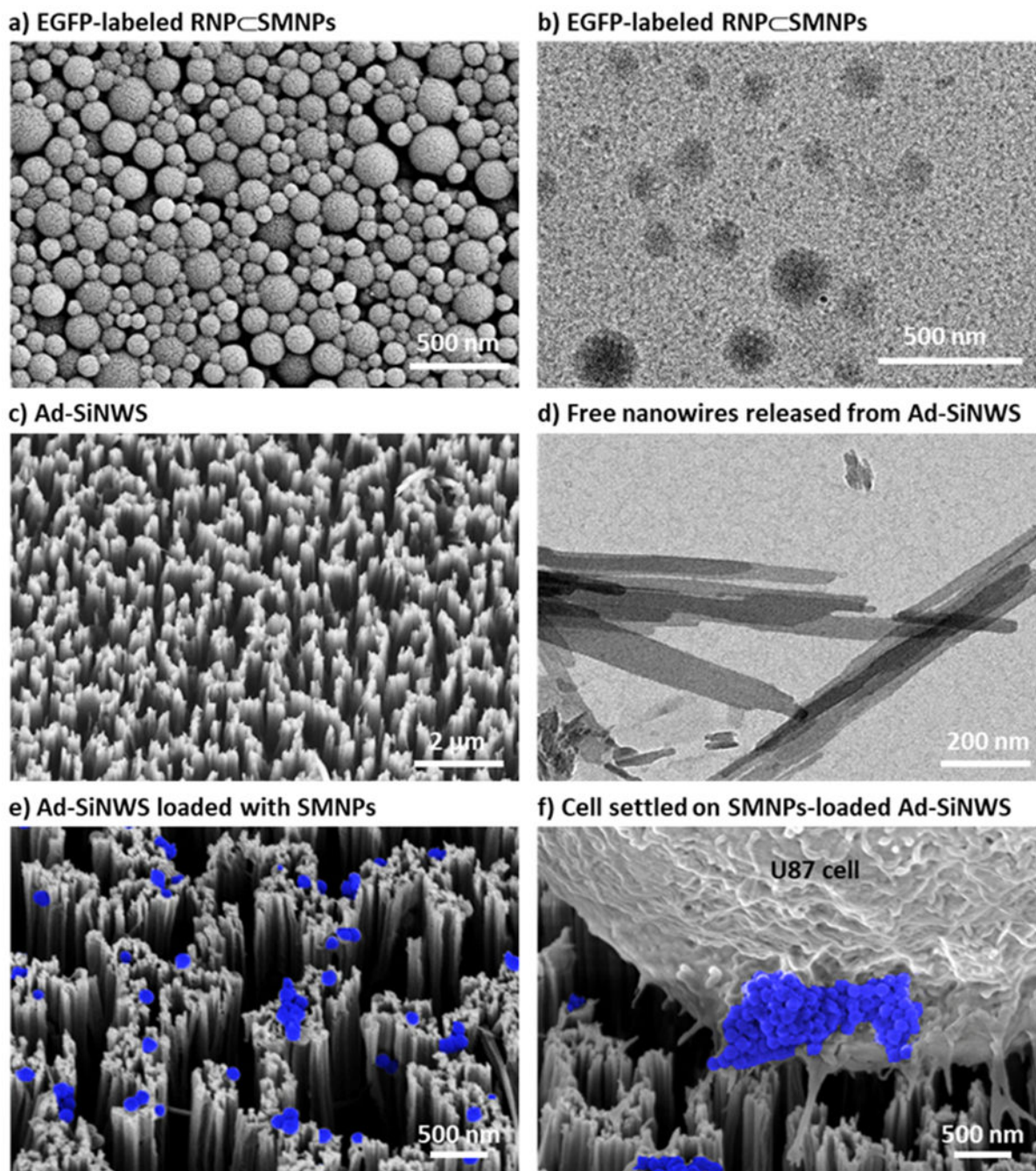


Figure 3.

a) Scanning electron microscopy (SEM) and of b) transmission electron microscopy (TEM) images of EGFP-labeled RNP-SMNPs. c) SEM image of Ad-SiNWS prepared *via* wet-etching followed by covalent functionalization of Ad motifs. d) TEM image of free nanowires. e) Upon exposure of SMNPs in the medium to the Ad-SiNWS, the SMNPs become grafted onto the Ad-SiNWS as indicated by SEM. The SMNPs are highlighted in false color (blue) to improve contrast. f) The interaction between a U87 cell and an Ad-

SiNWS loaded with SMNPs was visualized by SEM, where SMNPs are highlighted in blue (false color).

Author Manuscript

Author Manuscript

Author Manuscript

Author Manuscript

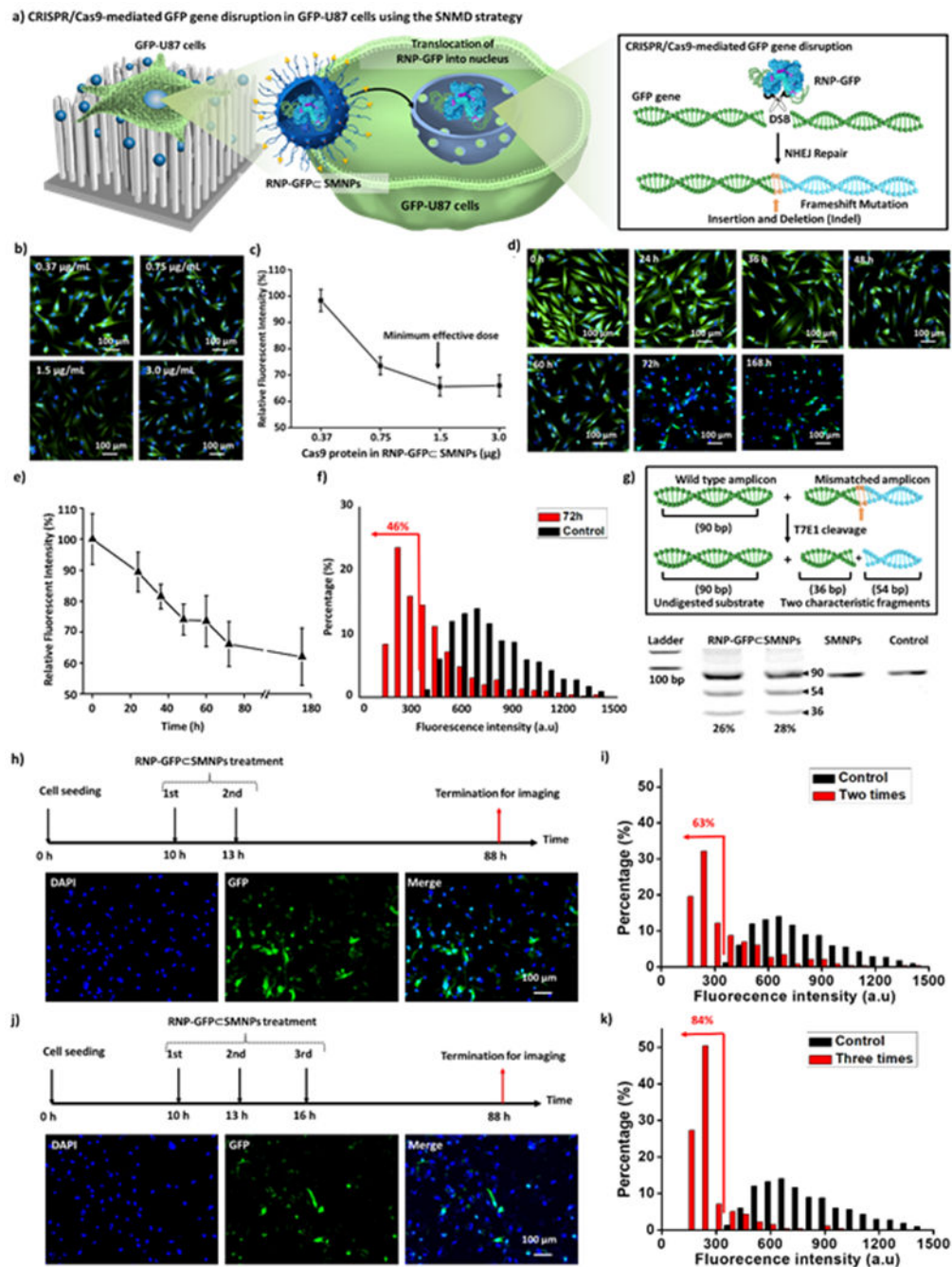


Figure 4.

a) Performing CRISPR/Cas9-mediated GFP gene disruption in GFP-U87 cells using SNMD strategy. The RNP-GFP:SMNPs were prepared by encapsulating RNP-GFP into an SMNP vector. **b)** Fluorescence micrographs of GFP-U87 cells collected at 48 h post GFP-U87 cell settlement. Four different Cas9 protein doses (0.375, 0.75, 1.5, and 3.0 $\mu\text{g}/\text{mL}$) in RNP-GFP:SMNPs were studied. **c)** Quantitative analysis of the fluorescent micrographs in b) shows dose-dependent disruption of the fluorescence signals in the GFP-U87 cells. A minimum effective dose is therefore determined as 1.5 μg of Cas9 protein per mL. **d)** Serial

fluorescence micrographs of GFP-U87 cells collected at 0, 24, 36, 48, 60, 72, 168 h post GFP-U87 cell settlement. **e)** Quantitative analysis of the fluorescent micrographs in d) shows the time-dependent decay of GFP signals. **f)** Histograms of GFP signals in individual GFP-U87 cells treated by RNP-GFPCSMNPs after 72 h, suggesting successful disruption of the GFP gene was achieved in 46% of GFP-U87 cells. **g)** T7E1 assay for detecting indel generation at the GFP gene in GFP-U87 cells treated with RNP-GFPCSMNPs (1.5 $\mu\text{g}/\text{mL}$ Cas9 protein) after 72 h. **h)** The designated timelines summarize the two sequential treatments of RNP-GFPCSMNPs to GFP-U87 cells *via* the SNMD strategy, sustaining a steady supply of RNP-GFP. Fluorescence microscopy images of GFP-U87 cells double-treated by RNP-GFPCSMNPs. Cells were visualized with DAPI (live/dead assay) staining (blue) and GFP expression (green). **i)** Histograms of GFP gene disruption performance in individual GFP-U87 cells double-treated by RNP-GFPCSMNPs after 88 h. **j)** The designated timelines and fluorescence microscopy images summarize the three sequential treatments of RNP-GFPCSMNPs to GFP-U87 cells. **k)** Histograms of GFP gene disruption performance in individual GFP-U87 cells triple-treated by RNP-GFPCSMNPs after 88 h. All data are presented as means \pm SD of three independent assays.

a) CRISPR/Cas9-mediated deletion of exons 45–55 of dystrophin gene in human cells using the SNMD strategy

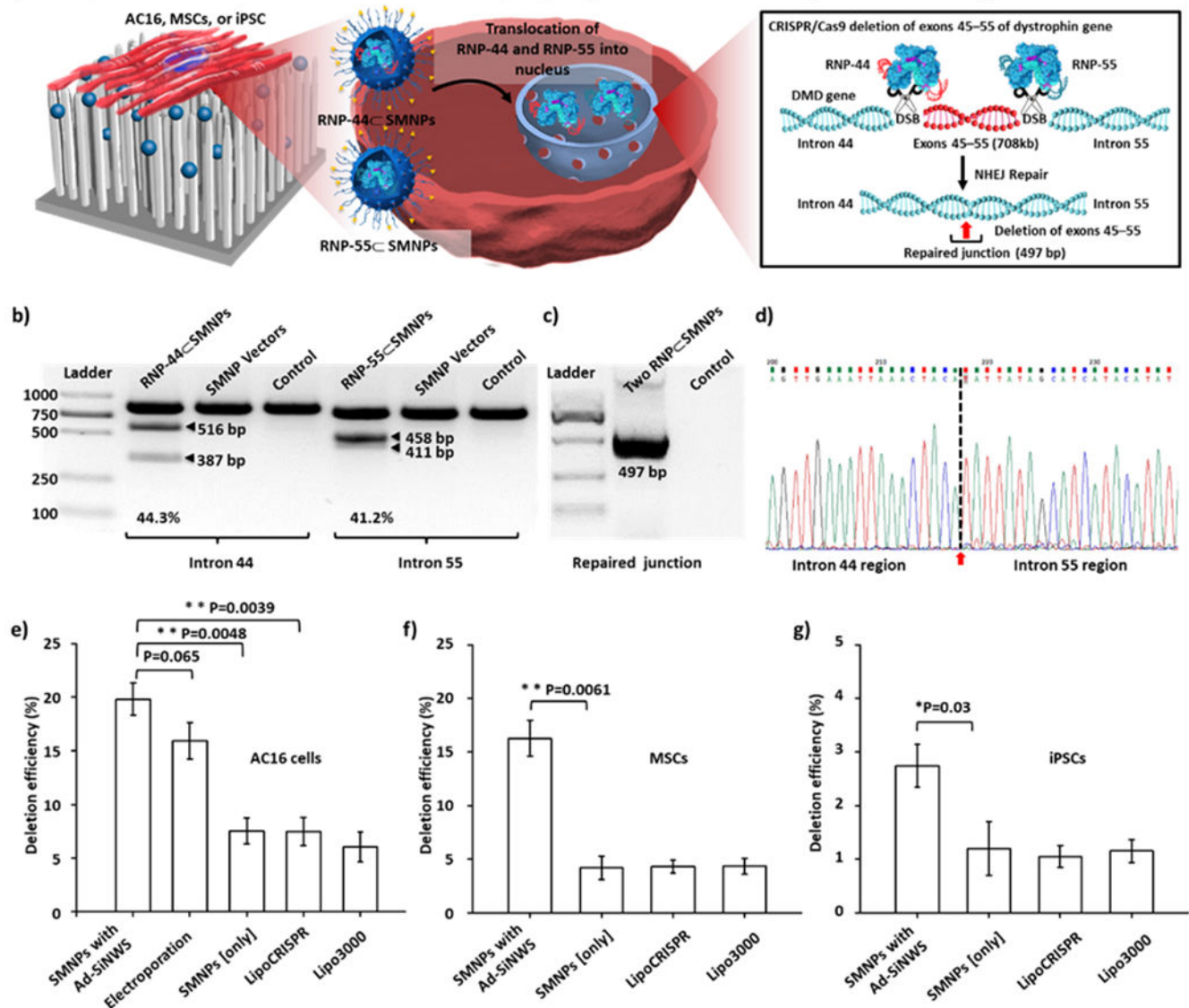


Figure 5.

a) Graphical summary for CRISPR/Cas9-mediated deletion of exons 45–55 of the dystrophin gene in the human cardiomyocyte cell line (AC16), induced pluripotent stem cells (iPSCs), and mesenchymal stem cells (MSCs) using the supramolecular nanosubstrate-mediated delivery (SNMD) strategy. Two RNP complexes (*i.e.*, RNP-44 targeting introns 44 and RNP-55 targeting introns 55) were separately encapsulated in SMNP vectors to give RNP-44CSMNPs and RNP-55CSMNPs. b) The T7E1 assay was used to determine the indel production efficiency at introns 44 and 55 of the dystrophin gene in AC16 cells triple-treated by RNP-44CSMNPs and RNP-55CSMNPs. c) A PCR assay and d) Sanger sequencing were used to confirm deletion of exons 44–55 of the dystrophin gene. e) Quantitative PCR for quantification of deletion efficiency in AC16 cells treated by SMNPs (RNP-44CSMNPs and RNP-55CSMNPs) with Ad-SiNWS, Electroporation (RNP-44 and RNP-55), SMNPs only without Ad-SiNWS, Lipofectamine CRISPRMAX

(RNP-44CLipoCRISPR and RNP-55CLipoCRISPR) or Lipofectamine 3000 (RNP-44CLipo3000 and RNP-55CLipo3000). f) Quantitative PCR for quantification of deletion efficiency in MSCs treated by SMNPs with Ad-SiNWS, SMNPs only without Ad-SiNWS, Lipofectamine CRISPRMAX, or Lipofectamine 3000. g) Quantitative PCR for quantification of deletion efficiency in iPSCs treated by SMNPs with Ad-SiNWS, SMNPs only without Ad-SiNWS, Lipofectamine CRISPRMAX, or Lipofectamine 3000. Data are presented as means \pm SD of three independent assays. A two-tailed unpaired t-test was used to determine the significance of the comparisons of data indicated in Figures e-f (*P<0.5, **P<0.01).

Author Manuscript

Author Manuscript

Author Manuscript

Author Manuscript